

DESIGN AND ENVIRONMENTAL TESTING OF THE DFKI-X ROBOTICS JOINT FOR SPACE APPLICATIONS

Niklas. A. Mulsow, Roland U. Sonsalla, Patrick Schöberl, Tobias Stark, and Frank Kirchner

DFKI Robotics Innovation Center, Robert-Hooke-Str. 1, 28359 Bremen, Germany

Email: {niklas.mulsow, roland.sonsalla, patrick.schoeberl, tobias.stark, frank.kirchner}@dfki.de

ABSTRACT

Within this paper we present the electro-mechanical development and testing of a highly integrated robotic joint. We are giving insight in the design of mechanical and electrical components and their evaluation with respect to a LEO mission. Furthermore, the model philosophy is described to adapt a joint, originally developed for terrestrial robots, to space qualification. The result is a novel and compact motor unit with integrated control electronics for space applications.

Key words: Robotic Joint, Space Actuator, Driving Unit, Driver Electronic, New Space.

1. INTRODUCTION

Future space missions show an increasing need for multipurpose, modular, but still compact and performant, actuation units. Past and current missions are using a wide variety of actuators. Typically, actuators and the associated control systems are mostly developed as separate elements for a specific use case. To reduce mission and development costs and to increase the actual short-term availability of actuator units for space applications, need arises for a highly integrated and performant robotic joint. The DFKI-X joints approach is promising to meet these demands and also to be beneficial for upcoming New Space applications.

Based on previous research [1], the further development of the DFKI-X joints motor-gear unit, motor electronics and control software is specified. The joint encompasses a torque optimized brushless DC motor in combination with a harmonic drive gearbox. To reach a high level of compactness hall- and temperature sensors are integrated in the motor unit. The design approach for the electronics is based on Commercial off-the-shelf (COTS) components which were specifically chosen to resist the space environment. It contains a flash FPGA with MRAM data storage as central processing unit, a GaN-FET power stage, a redundant designed ADC module and a CAN-Bus interface, hall sensor based trapezoidal and sensorless BEMF commutation and self-monitoring along with a latch-up protection for every function block. To show how the motor electronics can be integrated directly into

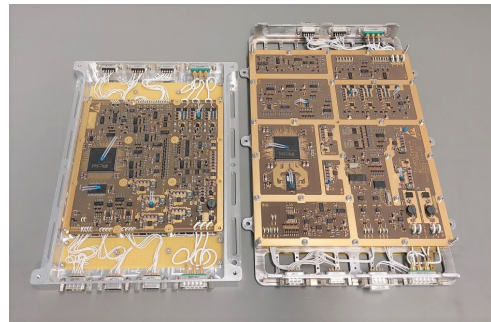


Figure 1. Electronics comparison: left EQM, right DM

the joint, the development model (DM) was significantly reduced in size (see Fig. 1) and different approaches for stacking individual functional blocks of the electronics were investigated. For evaluation, a structural-thermal model (STM) of the motor electronics was built and used during mechanical loads and thermal testing.

The qualification of the joint, including relevant environmental tests according to a LEO mission is described. A two-phase model and test philosophy was chosen, while the tests were in dependence on the ECSS standards. Qualification included thermal-cycling and thermal-vacuum, mechanical loads, including random and sine vibration, EMC as well as radiation tests with total ionizing dose and neutron irradiation. While tests have been successfully passed according to the focus of design and the LEO reference mission, different shortcomings and deficiencies could be observed during extended experimental tests. Besides the presentation of the robotic joint's design, results from qualification tests and lessons learned are discussed within the paper.

2. STATE OF THE ART

Table 1 provides a brief overview of prominent and up to date joints as used in space for orbital and planetary systems, while present development projects are outlined as well. The shown examples acknowledge the assumption that multipurpose robotic joints are a necessary ingredient of future space missions. Latest developments are the LARAD and the CAESAR, which are described below.

Table 1. Overview of robotic joints for space applications, [2], [3], [4], [5], [6]

Parameter	ROKVISS	IDD (azimuth)	LARAD (middle)	CAESAR Joint	DFKI-X Joint
duration	2005-2011	s. 2004	-	up 10y	12 - 14 month
usage	ISS	MER, Mars	ISS, LEO	LEO, GEO, Moon	TET-X, LEO
status	finished	in use	EM	EM under dev.	EM
motor	BLDC-TD	DC	BLDC	BLDC-TD	BLDC-TD
gear	HD	PG, HD	PG, WG, HD	HD	HD
reduction	160:1	8137:1	no ind.	no ind.	100:1
torque	40 Nm	45 Nm	129 Nm	80 Nm	22 Nm
speed	15 rpm	0,86 rpm	0,95 rpm	1,66	26 rpm
mass	2480 g	460 g	no ind.	no ind.	850 g
T_{op}	-20° to +30°	-70° bis +45°	k. A.	-20° to 60°	-20° bis +80°
controlled	FPGA	k. A.	MCU	FPGA/DSP	FPGA
sensors	TOR, POS, CUR, TEM ENC	MAS, ENC, POS, TEM	AS, ENC, POS, CUR, TOR, TEM, ACC	PS, TOR, CUR, TEM, ENC	CUR, TEM, ENC, AS
ACC:	acceleration sensor		POS:	output position sensor	
AS:	angle limitation		TEM:	temperature sensor	
CUR:	current		TD:	torque drive	
ENC:	motor encoder, incremental		TOR:	torque output sensor	
HD:	harmonic drive		DSP:	digital signal processor	
MAS:	mechanical stops		MCU:	micro controller	
PG:	planetary gearbox		WG:	worm gear	

The Lightweight Advanced Robotic Arm (LARAD) was developed on behalf of the United Kingdom Space Agency (UKSA) and in collaboration with a consortium of UK companies and manufactured at Airbus Defence & Space. The goal of the LARAD is to expand the capabilities and availability of long-range manipulators for in-orbit applications or planetary exploration. In that case, the manipulator will also provide a testbed for tooling trials. The newly developed manipulator can lift a 6 kg payload under 1 g of gravitational acceleration or use a 4 kg tool with 15 N reaction force. As a technology demonstrator, the latest technologies are used to manufacture the arm and joints (Fig. 2(b)).

With a similar purpose, the Compliant Assistance and Exploration SpAce Robot (CAESAR) was developed by DLR. Based on the RockViss joint, it represents a further development, whereby the mechanical set-up was only slightly changed. In terms of the position where the electronics are integrated, the arm represents a compromise, as they are not housed within the joint as in RockViss, but in a separate box at the base of the manipulator. The Joint (Fig. 2(a)) is designed for a variety of on-orbit services and a multi-purpose use like assembly, maintenance, repair, and debris removal receptive to LEO- and GEO-stationary missions [2].

Background DFKI X-Joint: The overall design and the integrated approach of the DFKI-X joint, as described in [1] is based on the iStruct joint, initially developed for the Charlie robot [7], and is the further advancement of the SpaceClimber joint, developed in 2007 [8]. Until today a wide variety of modular robotic joints has been developed for terrestrial and underwater robotic applications at DFKI RIC, spanning a range of nominal torque from 2.5 Nm up to 1000 Nm.

For development and qualification purposes, the TET-X



(a) CAESAR Joint [2]



(b) Joint of the Larad Arm [3]

Figure 2. Current joints under development for space robotics applications

mission requirements, as given in [9], have been used to define a reference mission. The key mission parameters and top-level requirements are according to a LEO mission with an altitude of 450 km, up to 850 km and a duration of 12-14 month. The rating for operations of the DFKI-X joint is derived from a sinusoidal load case which occurs on the shoulder joint of the DFKI's walking robot SpaceClimber while climbing within a 30° inclined slope and evaluated during experiments [10]. However, levels for radiation, thermal and vibration loads were tested also with higher values, as described in Sec. 7, for benchmark reasons and to pay regards to unknown lunch configurations and potential longer mission durations for further applications.

3. MODEL PHILOSOPHY

Based on experiences that the DFKI already has in previous described robotic applications, a hybrid philosophy, shown in Fig. 3 was chosen. The electronics is identified as critical element, hence, several tests were carried out

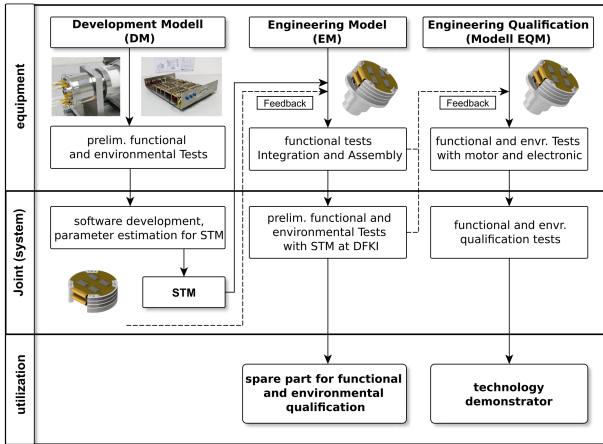


Figure 3. Model philosophy for reaching TLR 5

in advance for testing the suitability of available COTS components, as e.g. against radiation [1]. In addition, this made it possible to specifically investigate variants of circuits preliminary and select them for the EQM. Towards the envisaged integration to a compact joint, mechanical and thermal behavior of the electronic assembly with the motor unit could already be tested by using an STM. The model philosophy represents a reasonable compromise in terms of development time, risks and costs. On the following, the models and corresponding test results are further explained.

Development Model (DM): Two boards of the joint electronics in breadboard layout for the pre-development of software and for preliminary tests of the COTS components were built. On the mechanical side, a demonstrator was built with respect to form and function of the final design. Both served as first model for planned radiation and functional testing, parameter estimation, integration model, and for analysis and inspection. The knowledge gained from the setup and initial tests was used primarily to improve subsequent models and was incorporated into the development process.

Engineering Model (EM): The EM corresponds in form and function to the design of the EQM. The only exception is the gearbox, which is not certified for space use. The integration processes of the joints could be tested and practiced on the EM. The STM of the electronics can also be used for this purpose and the integration for the EQM can be tested.

Engineering Qualification Model (EQM): The EQM represents the final stage of the DFKI-X joint and was built up twice with one spare electronic PCB. That allows to perform extended tests like life-time and testing close to the expected maximum performance with high risk of destroying a unit. Additionally, it also allows conclusions to be drawn about differences that could be caused by manufacturing and integration. For investigating the integration of the electronics directly at the joint, its represented by an STM, which was also used during thermal

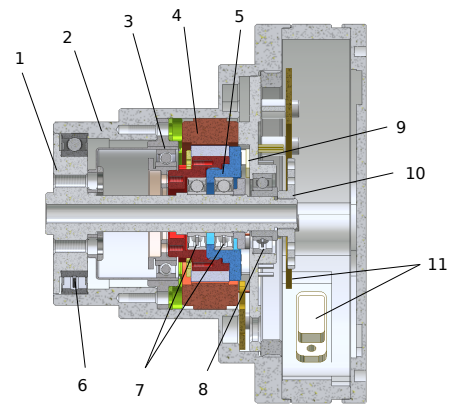


Figure 4. CAD representation of DFKI-X Motor-Gear Unit, 1: output shaft, 2: aluminium housing, 3: Harmonic Drive CPL-14-100-SP gearbox, 4: BLDC motor: Robodrive ILM 5008, 5: rotor unit with target ring (blue), 6,8 SBN four point bearing pair in O-arrangement, 7: SBN precision bearings for rotor in O-arrangement, 9: OMH3075B hall-sensors, 10: nut for adjustable output-bearing pre stress and targets for electric limit sensors, 11: cable routing and connectors

vacuum and vibration loads tests. The EQM was used to perform all critical environmental and functional tests on qualification level with appropriate margins.

4. MOTOR UNIT

Figure 4 shows the schematic design of the DFKI-X joint. The detailed construction is described in [1]. Derived from the DM, only minor changes were made to the EM and EQM. Regarding the overall stiffness, bearings were replaced with stronger ones of the same series and the shaft with its output side screw holes was strengthened to endure higher mechanical loads. Most obvious is the extension for routing the sensor cables to ECSS standards and for adding micro d-sub connectors. To set electrical limits and for calibration of the joints position, two hall sensors as for motor commutation were used (see Fig. 4). Targets integrated in the shafts end nut give feedback about the output position. The setups allows a resolution of 0.12° which is enough for the reference robotic use-case. The maximum outer diameter of 99 mm was chosen under considerations regarding integration of the electronics into a joint module. Compared to the DM of the joint, this increased the overall dimension, but it also underlines the need of downsizing approaches for electronics, described in Sec. 5, for future developments.

5. ELECTRONICS

The EQM joint electronics as shown in Fig. 5 is based on selected COTS components with adjustments to the design level of the DM, described in [1]. Figure 6 shows the schematic design of the functional building blocks. Without changing the basic performance parameters, the following changes were made at design level.

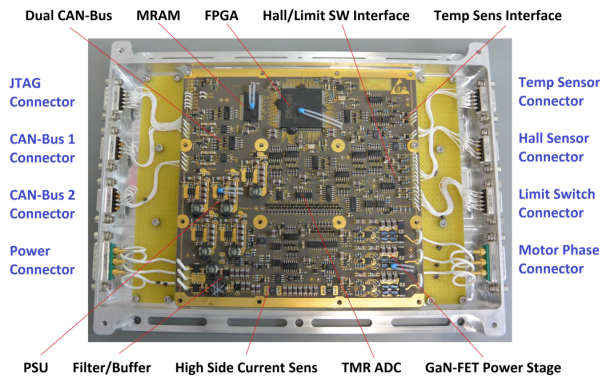


Figure 5. EQM of the highly integrated DFKI-X electronic unit

To prevent an undefined state for the GaN-FET power stage, the FPGA PWM signals to drive the motor phase were mirrored to a second FPGA I/O Bank and merged by discrete logic for realizing a self-testing of “Single event Upsets” at the FPGA I/O Banks. So non floating signal could reach the GaN-FET driver ICs such that the power stage always has been in a well-known mode. Also, the FPGA I/O Banks are coupled via some single I/Os to find out, if a single event upset happened. In addition, a triple redundant oscillator with FPGA voter was added after output level degradation was observed at the COTS oscillator under radiation during preliminary testing of the DM. Due to budget constraints, no different types of oscillators could be tested with respect to functionality under radiation. Leading to the decision to add three different COTS oscillators in parallel with different technologies (default CMOS, PECL/LVCMOS and MEMS type) with a software voter.

For keeping the assembly more compact, the two different CAN-Bus protocol controller were removed and replaced by FPGA software. Only the transceivers and their ESD/EMC protection circuitry were used, which saved components. Respective reducing the size of the board, the placement was realized double sided and more compact in comparison to the DM, shown in Fig. 1. It was possible to reduce the PCB size from 250x200 mm (DM) to 160x160 mm (EQM) without changing performance parameters.

5.1. Structure and Thermal Modelling of a Folded and Integrated Joint Electronic

The development of the current electronics for the DFKI-X joint (Fig. 5) has so far been carried out separately at the layout level from the integration into the DFKI-X joint. However, the goal is as described above a further minimization of the dimensional area of the electronics for a sufficient integration to a compact unit. For that, the STM replicates the electronics closely in terms of mass and the thermal properties. As a result, testing during the verification process (Sec. 7) will provide data that will allow conclusions to be drawn about the integrability of the electronics into the joint and serve as a basis for

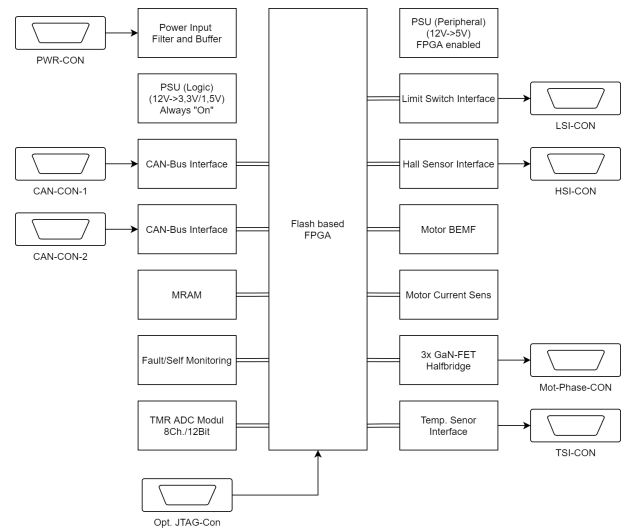


Figure 6. Electronic functional blocks

future developments. Figure 7 shows the assignment of the functional building blocks and the principle design of the electronics STM.

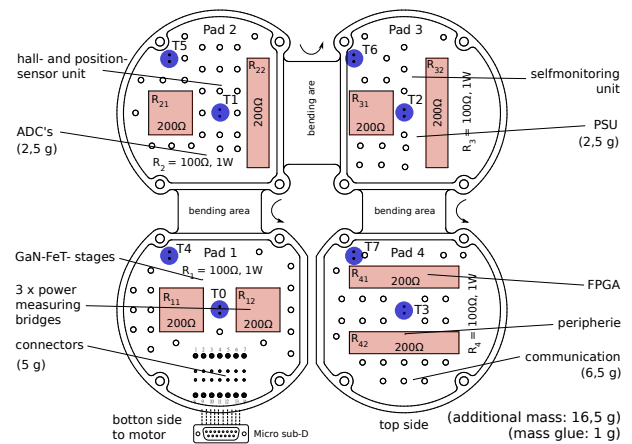


Figure 7. Functional blocks assignments

To realize the fusion of electronics and mechanics with minimal installation space, a solution for a 3 dimensional arrangement of the electronics was searched for. Different mechanical concepts and methods for connecting the divided boards to the DFKI-X joint have been investigated. Mechanical stiffness, thermal coupling, lightweight design aspects and the routing capabilities have been driving factors for the selection. During analysis it turned out, that the amount of connectors would not allow to use plugs or cable connections because of space restrictions. A semi-flex PCB design was chosen, which provides a homogeneous layer structure and a solid manufacturing while cost remains low. Disadvantages such as the bending radius of 5 mm are compensated by the fact that this distance is required anyway for higher electrical parts. The area of the current electronics, which corresponds to 256 cm², could be accommodated on the flex-PCB with a diameter of 95 mm, by four boards. The

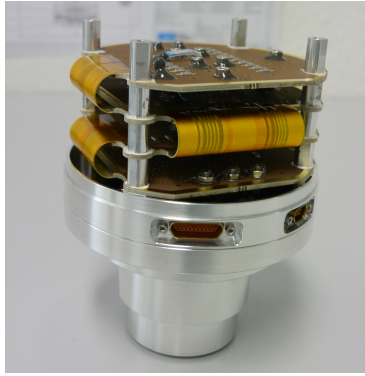


Figure 8. Fully integrated EQM of the Joint with STM

mechanical structure was designed with respect to a maximum thermal load of 4 W at heating by a gradient of 8 K to the center of the PCB compared to the housing. These values were estimated at the first radiation loads tests with the DM of the electronics, considering the degeneration due to the lifetime. The housing was designed with a wall thickness of 1.5 mm aluminium. Due to its round shape, it has high stiffness in all spatial directions. The lowest natural frequency analyzed was 515.25 Hz. Electrical parts are replicated by additional masses for the vibration loads tests. The electrical power losses could be simulated by resistors while temperatures were measured for each board near the mounting side and in the center to get a detailed look into the thermal behavior during thermal vacuum testing. The assembled STM with the DFKI-X joint is shown in Fig. 8 and was used during mechanical and thermal-vacuum tests, as described in Sec. 7.

6. SOFTWARE DESIGN

To reduce development time and cost the software to drive and test the DFKI-X joint was build up on the software used in almost all motors at the DFKI RIC as already described in [1]. This software uses the NDLCOM protocol [11] which facilitates a flexible low-level communication with minimal overhead and is therefore suited for the use within the DFKI-X joint.

As mentioned in Sec. 5 the CAN-Bus controllers were removed in the redesign of the electronics and a minimal CAN-Protocol stack was implemented within the FPGA. To obtain a reliable clock signal a TRM module was implemented which tries to recognize degradation of the oscillators. A second TRM module was used to verify the output signals of the different ADCs. Also an error handling was implemented which uses the self-monitoring capabilities of the electronics as well as normal error detection as it is used in other joints (e.g. temperature and current limits or plausibility tests of input signals).

For testing, a widget to enable and disable the different function blocks of the electronics was implemented to check them separately during the runs.

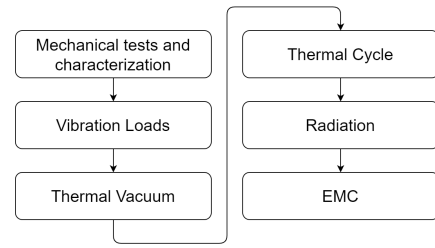


Figure 9. Basic sequence of key tests for the EQM

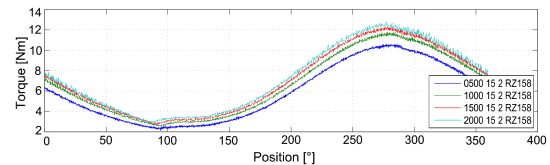


Figure 10. Load curve used for the joint in following tests, depending on rotation speed

7. TESTS

The test strategy was chosen to meet the required reference mission parameters as well as to determine the performance and maximum duration of the components. The test sequence, shown in Fig. 9, was preceded by various pre-tests [1]. Each test is divided into separate runs and levels, between each environmental test the joint was subjected to functional tests. Destructive designed tests, such as the radiation test, were performed with additional space models. Within the environmental tests, the load curve shown in Fig. 10 was used. In spite no lifetime tests was performed, the EQM of the joint itself reached during the campaign more than 40,000 revolutions. [12]

7.1. Vibration Loads

The test setup for the vibration loads test is shown in Fig. 11. The sensors measure the resulting acceleration at tests specimens. Measuring points were: At the rear of the STM, at the output of the shaft and on the top of the electronics housing in the center. The positions were chosen to monitor the parts with the expected highest deflection during test and/or critical parts where low deflection is required, as the output shaft.

The parameters for qualification level are shown in Table 2. Since the test parameters for payloads below 10 kg are not specified for each launcher and they differ significantly from the requirements for heavier payloads, the test parameters from the Space Shuttle [13] (random Vibration 01) and the calculation formula according to ECSS-E-10-03A (random Vibration 02) were chosen. The sinusoidal run corresponds to the values for payloads below 50 kg according to the requirements of ECSS-E-10-03A. In general, due to the low mass of the joint, the selected test parameters for the vibration level, especially those according to ECSS-E-10-03A, can be classified as very high and above the requirements of the TET-X ref-



Figure 11. Mounting of the DFKI-X Joint with STM and electronic on shaker

Table 2. Vibration loads

run	parameters	intensity	duration
resonance search	20 - 2000 Hz	0,5 g	2 oct per min $\hat{=}$ 200 s
sine vibration	5 - 21 Hz 21 - 60 Hz 60 - 100 Hz	11 mm 20 g 6 g	2 oct per min $\hat{=}$ 200 s
random vibration 01	20 - 50 Hz / +3 dB/oct 50 - 600 Hz 600 - 2000 Hz / -3 dB/oct	0,025 g ² /Hz at 20 Hz 0,15 g ² /Hz 0,025 g ² /Hz at 2000 Hz (12,9 G _{rms})	2 min per axes
random vibration 02	20 - 100 Hz / +3 dB/oct 100 - 300 Hz 300 - 2000 Hz / -5 dB/oct	0,19 g ² /Hz at 20 Hz 0,525 g ² /Hz 0,11 g ² /Hz at 2000 Hz (18,2 G _{rms})	2 min per axes

erence mission [14]. For the verification, this means that flying with any available launcher would be in principle possible. However, the lunch configuration has always to be considered specially.

All runs passed successfully. Notable was, that the motors noise and current consumption decreased significantly after first vibration tests performed. It may be due to a reduction of stress within the pre-stressed bearings. However, no noticeable backlash was observed at the joint after all vibration tests finished. Nevertheless, the effect should be further investigated for future developments to ensure that no negative impact is verifiable. The lowest eigenfrequency measured at the STM was at 449.5 Hz. The value agrees well with analysis results, since the influence of the three measurement sensors is not negligible to the light structure. The analysis was repeated including the measurement sensors and cables mass with a deviation of less than 10%.

7.2. Thermal Vacuum and Cycling

For testing under thermal and vacuum conditions, the joint was operated repetitively. In the first cycle, the joint was operated under short-time duty at 30-minute inter-

Table 3. Parameters for thermal vacuum testing, Values in brackets: second run, TNO: temperature non operating, TSU: temperature at switch ON, TOP: temperature operational

ambient	qualification	experimental
TNO-max	65	110 °C
TSU-max	60	85 °C
TOP-max	50	80 °C
TNO-min	-30	-40 °C
TSU-min	-25	-35 °C
TOP min	-20	-30 °C
hold duration	2 h	2 h
stability	1 K/h	1 K/h
vacuum	10 ⁻⁵ hPa	10 ⁻⁵ hPa

joint	parameters
Load	3-15 Nm
T-On/Off	10/30 min
rotation speed, (cycle 1)	20 to 200 °/s
rotation speed, (cycle 2-8)	10 to 80 °/s (reduced)
STM-On	0,8/1,6 W

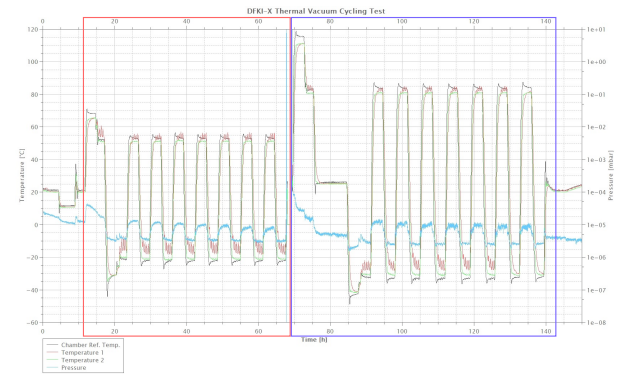


Figure 12. Overview thermal cycle, red: values for TET-X Mission, blue: experimental values

vals. This allowed to adjust the motors temperature to the chambers temperature during idle periods. The second cycle was performed under continuous operation at 35% of the maximum power. The test passed successfully except for an error in low-voltage measurement in software. Table 3 sum up the test parameters. In Fig. 12 the whole test sequence is shown.

During the tests, the STM was used for further investigation of electronics thermal behavior (Sec: 5.1) during thermal cycling tests. Figure 13 shows the detailed course of the heating curves from the joint and the STM during operation in the warm phase of the first thermal cycle. The power-up phases, during which the motors velocity profile was active, are labeled with T_E. The blue line shows the motors temperature, measured at the stator. The red line (STM-T0) corresponds to the temperature sensor in the center at the motor-side at PAD 1 (c.f. Fig. 7). The yellow line (STM-T3) corresponds to the temperature in the center of the uppermost PAD 4. The chosen locations and plotted values were selected based on the most critical behavior. The diagram be-

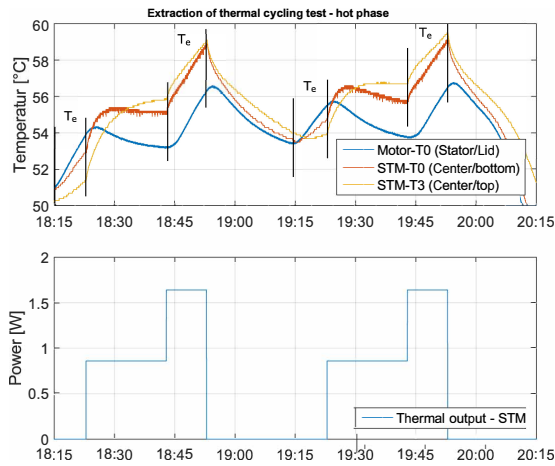


Figure 13. Temperature of the DFKI-X Joint and selected sensors of the STM during testing at warm phase. Below: STMs peak power, congruent with motor is running

low shows the corresponding power profile of the STM. It can be seen, that the maximum deviation of the temperature curves from the STM and the motor in this experiment was 2.3 K, which is very much within a feasible range. The maximum total temperature was 59° C. Since the current electronics for the DFKI-X joint are designed for a temperature range of -30° C to +80° C, it can be assumed that electronics with the same shape and physical properties as the STM are feasible, according to the given requirements to reference mission and parameters above.

7.3. Radiation

The radiation tests were split into separate pretesting with the DM as described in [1] and the final tests with the EQM. Both tests were set up as potentially destructive and were performed until the maximum achievable limit. While first tests served to classify the DM electronics and to see which functional blocks are most sensitive, second tests performed according to ESCC 22900 to reach the 10krad level described below. Table 4 showing the parameters for the first tests runs, passed successfully after all required mission key parameters for a 14 month 850 km LEO reference mission, and showed good performance for COTS components. The last run was ended while motor an log-data still running, but failed when trying to reconnect after switching off the joint.

Table 4. Parameters at the radiation pre-test, Shielding 3 mm Al, NR: neutron radiation at 14 MeV no shielding

Run	Rate	Total dose	Res.
TID 01	0,345 krad/h	2,7 krad	P
NR 01	0,233*10 ¹⁰ N cm ⁻² h ⁻¹	0,43 10 ¹⁰ N cm ⁻²	P
NR 02	0,233*10 ¹⁰ N cm ⁻² h ⁻¹	1,21 10 ¹⁰ N cm ⁻²	P
TID 01	0,345 krad/h	5,0 krad	P
TID 02	0,345 krad/h	9,9 krad	P
TID 03	1,068 krad/h	16,9 krad	P
TID 04	1,068 krad/h	32,8 krad	F

Table 5. Parameters at the radiation final test, Shielding 3 mm Al, NR: neutron radiation at 14 MeV no shielding

Run	Rate	Total dose	Res.
NR 01	0,34*10 ¹⁰ N cm ⁻² h ⁻¹	1,74 10 ¹⁰ N cm ⁻²	P/F
TID 01	0,36 krad/h	5 krad	P
TID 02	0,36 krad/h	10 krad	P
TID 03	0,36 krad/h	15 krad	P
Annealing	-	24h	-
TID 04	0,36 krad/h	20 krad	P
TID 05	0,36 krad/h	45 krad	F

After a PCB update, as specified in Sec.5, final testing according to ESCC 22900 with the final EQM were performed. For TID testing a lower dose rate was chosen and an additional annealing after the 15 krad step was included. Table 5 summarized the performed runs during the TID tests. During all test runs the joint was operated under short term operation (10 min on / 20 min off) while a maximum power of 80 W was retrieved at maximum.

During neutron radiation testing, triggering of various voltage protectors were observed. However, resetting per software led into continuing the run without noticeable failures of the boards voltages and performances. After transfer to TID test chamber a restart of the board was not possible and needed to be replaced. During TID tests no significant current increase on the logic power supply was observed. The PC to board communication failed once during test period between 15 krad and 20 krad, but tests could be continued after a soft reset. During the 20 to 40 krad step the board communication was interrupted while log data was still transmitted and FPGA ID query via JTAG was still possible. However, reloaded failed because of probably defective internal voltage converter in the FPGAs VPump.

7.4. EMC

EMC testing for the DFKI-X joint was performed in accordance with requirements for ECSS-E-ST-20-07C. Despite precautions, the test regarding cable bound EMC have not been passed as it was figured out that some points have to be focused on for further developments. Besides improvements on electronic hardware side, which means basically a better shielding of sensors and cables.

An identified problem is based on the use of GaN-FETs and there switching speed. Currently a PWM speed of about 30 kHz (time-base 33μs) is used but the used GaN-FETs would change their state in less than 10 ns which causes for the joint some EMC trouble in range of 2-4 MHz with slightly more than 50 dbμA common mode noise at the motor phases, although a snubber network and freewheeling diodes were used next to the GaN-FETs. To reduce this disturbance, an output filter (like an L-C filter) right after the GaN-FET power stage, a shielded housing and shielded motor phase cables are required. To minimize the physical output filter size, an in-

crease of the 30 kHz PWM to about 100-200 kHz and a sinus commutation instead of a block commutation would be advisable.

8. CONCLUSION AND OUTLOOK

The DFKI-X robotic joint, as presented in this paper, represents a highly integrated joint module for robotic applications in space. A series of functional and environmental tests have been performed with very promising results. The first iteration of miniaturization of the joint electronics as well as tests with the STM have shown how a possible design of compact control electronics can be realized mechanically and thermally in the future.

Using COTS components has been beneficial for integrated functions due to the fact, that more advanced components and ICs are available than traditional space components. The used P-FET based over current protection circuit in a very small footprint is such a positive example. Also, fully automotive qualified GaN-FETs and gate drivers have been turned out as excellent and compact alternative for realizing power circuits. For the next evaluation steps, critical parts should be early identified and pre-qualified. Also, COTS parts should be ordered in high quantities and stored to expand the product life cycle.

All required mission key parameters, except some solvable issues while EMC testing for an up to 14 month 850 km LEO were observed and passed. Testing on higher levels, such as done for thermal vacuum and radiation loads, promises a well suited performance of the joint, which could help to bring robotic applications easier into space. The performed tests with the folded electronics STM have shown the feasibility and potential for further miniaturization of joint electronics. However, it has to be discussed on system level, to figure out what the best approach will be for combining the mechanical and electrical parts of the robotic joint. This aspects along with a general modularization approach will be further investigated in the future. It is envisioned to build up on the current breadboard design and the STM pre tests to combine all elements into one modular robotics joint unit. The joint will be part of a standardized robotics toolbox which is currently under development and is proposed to be fully qualified for space applications in the near future.

ACKNOWLEDGMENTS

The authors would like to thank the TransTerra team and all supporting staff at DFKI Robotics Innovation Center Bremen. The work presented is part of the projects TransTerra (grant no. 50 RA 1301) and MODKOM (grant no. 50 RA 2107) which are funded by the German Space Agency (DLR Agentur) with federal funds of the Federal Ministry of Economics and Technology in accordance with the parliamentary resolution of the German Parliament.

REFERENCES

- [1] R. Sonsalla et al. DFKI-X: A Novel, Compact and Highly Integrated Robotics Joint for Space Applications. In *Proc. of ESMATS 2017: 17th European Space Mechanisms and Tribology Symposium*, Hatfield, England, September 2017. VDE.
- [2] A. Beyer et al. Caesar: Space robotics technology for assembly, maintenance, and repair. In *69th International Astronautical Congress (IAC)*, Oktober 2018.
- [3] E. Allouisa et al. Larad – architecture and implementation of a lightweight advanced robotic arm demonstrator for future space and planetary applications. In *14th Symposium on Advanced Space Technologies in Robotics and Automation*, June 2017.
- [4] E. T. Baumgartner et al. The Mars Exploration Rover instrument positioning system. In *Proc. of the 2005 IEEE Aerospace Conference*, pages 1–19, March 2005.
- [5] A. Wedler et al. Robotic components for space rovkiss and dextrand. In *Proc. of the International Conference on Robotics and Automation (ICRA)*, May 2011.
- [6] A. Wedler et al. DLR's dynamic actuator modules for robotic space applications. In *Proc. of the 41st Aerospace Mechanisms Symp.*, Mai 2012.
- [7] D. Kühn et al. System design and testing of the hominid robot Charlie. *Journal of Field Robotics*, April 2016.
- [8] J. Hilljegerdes et al. Development of an intelligent joint actuator prototype for climbing and walking robots. In *Proc. of the 12th Int. Conf. on Climbing and Walking Robots and the Support Technologies for Mobile Machines (CLAWAR)*, 2009.
- [9] W. Moldenhauer et al. TET-X user manual for payloads. Technical Report TET-KTH-UM-003, Kayser-Threde, January 2011. Issu 2.
- [10] S. Bartsch et al. Development of the six-legged walking and climbing robot SpaceClimber. *Journal of Field Robotics*, 29(3):506–532, May/June 2012.
- [11] M. Zenzes et al. NDLCOM: Simple protocol for heterogeneous embedded communication networks. In *Proc. of the Embedded World Exhibition and Conference*, Nürnberg, Germany, February 2016.
- [12] N. Mulsow. Beitrage zur Verifizierung des DFKI-X Gelenkes für den Einsatz im Weltraum. master thesis, Universität Bremen, 2017.
- [13] Special Payloads Division Goddard Space Flight Center. *Get Away Special, Small Self-Contained Payloads an Experimenter Handbook*, 1 edition, 1985.
- [14] W. Moldenhauer. *TET-X, User Manual for Payloas*. Kayser-Threde GmbH, 2 edition, Januar 2011.